2024

Shock Tube Ignition Studies of Renewable Diesel Fuels for Medium and Heavy-Duty Transportation

Zuhayr Pasha Mohammed
University of Central Florida

SHOCK TUBE IGNITION STUDIES OF RENEWABLE DIESEL FUELS FOR MEDIUM AND HEAVY-DUTY TRANSPORTATION

by

ZUHAYR PASHA MOHAMMED
Bachelor of Science in Mechanical Engineering, University of South Florida, 2022

A thesis submitted in partial fulfillment of the requirements
for the degree of Master of Science
in the Department of Mechanical and Aerospace Engineering
in the College of Engineering and Computer Science
at the University of Central Florida
Orlando, Florida

Spring Term
2024

Major Professor: Subith Vasu

ABSTRACT

Currently extensive research on alternative fuels is being conducted due to their increasing demand to reduce greenhouse emissions. One renewable fuel studied in this work is dimethyl ether (DME) blended with propane(C_3H_8) as a potential mixture for heavy-duty engines used in semi-trucks. The blend has the potential to drastically reduce particulate and greenhouse gas emissions compared to a conventional diesel engine operating under similar conditions. To develop the use of mixture, one must conduct detailed conceptual and simulation studies before progressing to detail studies in CFD, engine modifications, and live testing. For simulations, accurate high-fidelity chemical kinetic models are necessary. However, the validity of the chemical kinetic mechanism for operating conditions of a heavy-duty mixing-controlled compression (MCCI) engine was widely unknown until recent work presented here and published. In this work, we studied the ignition of DME and propane blends in a shock tube under MCCI engine conditions. Ignition delay time (IDT) gathered behind the reflected shock for DME-propane mixtures for heavy-duty compression ignition (CI) engine parameters. Testing was conducted for undiluted varieties spanning from temperatures of 700 to 1100 K at pressures ranging from 55 to 84 bar for various blends (100% CH_3OCH_3, 100% C_3H_8, 60% CH_3OCH_3/ 40% C_3H_8) of DME and propane were combusted in synthetic air (21% O_2/ 79% N_2). Several experiments were conducted at higher pressures (90-120 bar) to improve the model performance and accuracy. The ignition delay times (IDTs) were compared to recent mechanisms, including Aramco3.0, NUIG, and Dames et al. A common trend among the mechanisms was overpredicted experimental IDTs. Further studies were conducted by a sensitivity analysis using the Dames et al. model, and critical reactions sensitive to IDTs of DME-propane mixture near 60 bar are outlined. Chemical analysis was conducted on the NTC region to explain chemical kinetics which is critical for developing MCCI heavy duty engines.

This dedication goes out to my parents Afzal and Rehana who have been supportive of my pursuit of higher education.

ACKNOWLEDGMENTS

I would like to thank my advisor Prof. Subith Vasu who has given me the opportunity to conduct this research to further advance my career and to leave a positive impact on the environment in years to come. My lab manager Dr. Justin Urso has also been a great support in the whole process throughout my entire educational and research experience at UCF. Providing insight into all experimental aspects of my project. Dr. Ramees Rahman taught me the chemical background I needed for the computational side of my project which allowed me to gain a deeper understanding of the chemical processes occurring during experimentation.

This material is based upon work supported by the U.S. Department of Energy's Office of Energy Efficiency and Renewable Energy (EERE) under Award Number DE-EE0009879. Partial support from the University of Central Florida is also acknowledged.

TABLE OF CONTENTS

LIST OF FIGURES

LIST OF TABLES

CHAPTER ONE: INTRODUCTION

In 2019,in the U.S. the second-largest energy consumer after the industrial sector is the transportation sector, consuming roughly 28 quadrillion BTUs (British Thermal Units) (quads) [1]. In 2022, the global carbon dioxide emissions from the transportation sector increased by 254 megatons [2]. For the United States Region, the projected transportation energy consumption is 28.2% in 2024 compared to all combined major industrial, residential, commercial, and transportation sectors [1]. The rise in the global energy demand and temperatures has been driving the industry to implement alternatives to petrol and diesel fuels, which are significant contributors to greenhouse gas (GHG) emissions. One possibility to replace diesel and petrol is liquid petroleum gas (LPG) [3], consisting of ~80-100% propane. Also, storage and transportation of propane can be easily implemented due to the existing infrastructure [4] for its constituents. Propane also has a significant energy content (LHV = 46.4 MJ/kg) [5], which surpasses both petrol (43.2 MJ/kg) [6] and gasoline (43.4 MJ/kg) [7]. Despite propane's high LHV, it must be blended with another fuel due to its lower cetane number Table 1, enhancing its autoignition characteristics [8]. One biofuel is dimethyl ether (DME, 28.43 MJ/kg) [5].

Table 1: Properties of Relevant Fuels

Fuel	**Cetane Number**	**Lower Heating Value (MJ/kg)**	**Autoignition Temperature (K)**
Diesel	40-55 [5]	42.5 [5]	523 K
LPG (C_3H_8)	5 [5]	46.4 [5]	743 K
DME	55-60 [5]	28.4 [5]	508 K
Gasoline	-	43.4 [7]	519 – 553 K [7]

DME is the simplest ether, a renewable-based alternative fuel that does not contain any C-C bonds in its chemical makeup; this allows DME to have near-zero soot-free combustion [9]. It is also a non-toxic, non-carcinogenic, non-teratogenic, and non-mutagenic fuel. However, DME must be well characterized as it is very flammable, and incomplete combustion will produce toxic emissions. Due to DMEs inert combustion properties, engines can utilize higher exhaust gas recirculation to reduce nitrogen oxide emissions without regard to the NOx–soot trade-off. Due to DME having similar combustion properties to diesel, it is also considered a drop in fuel for diesel with minor modifications to fuel systems and storage, where DME has a vapor pressure similar to LPG, so similar storage units can be used [10].

Additionally, the fuel and oxidizer are not premixed in an MCCI engine and might encounter a wide range of equivalence ratios ranging from very lean ($\Phi < 0.2$) to very rich ($\Phi > 2.0$) [11]. The chemical kinetic models developed for CFD simulations of MCCI engines must capture all these conditions. To validate chemical kinetic mechanisms generated for propane-DME chemistry, high-pressure measurements are required for the fuel's IDT at a range of equivalence ratios and temperatures encountered by a MCCI engine. The shock tube reactor is an ideal device for generating a high-pressure environment and has been used for studying combustion since the 1940s [12]. Shock tube experiments assume homogeneous distributed quiescent gas behind the reflected shock, with test times on the order of a few milliseconds. This enables comparison of kinetic model predictions to experimental data from shock tube experiments, assuming constant internal energy and volume [12].

CHAPTER TWO: LITERATURE REVIEW

Table 2 shows a majority of studies that are focused on ignition delay time measurements while even soot yield from 1800-2600K at 5 atm have been researched for propane [13]. For blends of propane and DME, IDTs have been published up to pressures of 50 atm [8] by Dames et al. CI engines operate at pressures of 30 – 70 bar [14], while heavy-duty engines used to power freight or semi-trucks operate at much higher pressures of around at least 100 bar. Currently, in literature, at higher pressures, there is a gap in knowledge on the ignition delay times of propane-DME mixtures at elevated pressures relevant to the combustion of heavy-duty engines. Few studies provided in situ, time-resolved measurements of key intermediate species to develop a high-fidelity chemical kinetic mechanism is missing unless it is the authors published work [15] and IDTs are now present in the results section of this work for a blend of DME/Propane.

Table 2: Showing a combination of recent studies of DME from many facilities.

Fuel	**Additive**	**T (K)**	**Pressure (Bar)**	**Source**	**Facility**
C_3H_8	DME	700-1100	54-83; 89-118	IDT [15]	Shock Tube
C_3H_8		689-1700	20-89	IDT [16]	Shock Tube & RCM
C_3H_8	DME	1100-1500	5-15	IDT [17]	Shock Tube
C_3H_8		1800-2600	5	IDT [13]	Shock Tube
C_3H_8		930-1070	9-11.4	IDT [18]	RCM
DME		468	3-6	IDT [19]	Spherical Chamber
C_3H_8		1043-1778	17.9-43.4	IDT [20]	Shock Tube
C_3H_8		1200-1600	1-10	IDT [21]	Shock Tube
DME	H_2	373	1	LBV [22]	Heat Flux Setup

DME		400-1100	1	IDT [23]	PFR
DME		555-1250	10-40	IDT [24]	CT-RCEM

CHAPTER THREE: MATERIALS AND DISCUSSION

HiPERSTAR Shocktube Facility

The ignition delay times gathered at the University of Central Florida's (UCF) High-Pressure Extended Range Shock Tube for Advanced Research (HiPER-STAR) facility [25, 26]. This newly built facility has been designed to withstand pressures reaching 1000 atm and can replicate combustion test conditions (T_5 and P_5) in a controlled environment.

The long stainless-steel shock tube is split into two sections. The high-pressure driver(P_4) and low-pressure driven side(P_1) as seen from Figure 1. Initially both sides of the Shocktube are vacuumed separately. The low-pressure driven side is vacuumed more rigorously by utilizing a series of vacuum pumps comprised of Agilent dual stage rotary cane pumps (DS 102) and a Kurt J, Lesker, TRIVAC B two-stage rotary vane pump (D8B), and an Agilent turbomolecular pump (TwisTorr 305 FS). This is to ensure that no impurities exist in the test section. The homogeneity of the mix is provided by Pairs of Neodymium nickel-coated magnets coupled to the motor to an impeller which stirs the mixture. The test mixture is then inserted based on Shocktube relations used to reach test conditions of P_5 and T_5.

The T_5 and P_5 are calculated using modified shock equations using the incident shock velocity (from pressure transducers) and driven conditions set during the experiment. This allows us to reach the initial conditions needed to achieve the targeted P_5 and T_5 found by the modified FROzen Shock code (RGFROSH) *[27]* using equations (2) and (3). The HiPERSTAR shock tube has a space reduction at the cross-section. This allows for an alternative way of heating the driver gas by producing a stronger shock. To account for the space reduction in experimentation, a correction factor (g) given by equation (4) must be applied to initial pressure ratio of P_4/P_1 using equation (1) [28].

$$\frac{P_4}{P_1} = \frac{2\gamma_1 M_1^2 - (\gamma_1 - 1)}{\gamma_1 + 1} \left\{ 1 - \frac{\gamma_4 - 1}{\gamma_1 + 1} * \frac{a_1}{a_4} \left(M_1 - \frac{1}{M_1} \right) \right\}^{-\left(\frac{2\gamma_4}{\gamma_4 - 1}\right)} \quad (1)$$

$$\frac{P_5}{P_1} = \left\{ \frac{2\gamma M_1^2 - (\gamma - 1)}{\gamma + 1} \right\} \frac{(3\gamma - 1)M_1^2 - 2(\gamma - 1)}{(\gamma - 1)M_1^2 + 2} \quad (2)$$

$$\frac{T_5}{T_1} = \frac{[2(\gamma - 1)M_1^2 + (3 - \gamma)][(3\gamma - 1)M_1^2 - 2(\gamma - 1)]}{(\gamma + 1)^2 M_1^2} \quad (3)$$

$$\frac{a_4}{a_1} g^{(\gamma_4 - 1)/2\gamma_4} \quad (4)$$

Splitting the two sections of the Shocktube is an Al diaphragm. After the test mixture, inert gases which do not interfere or react with the test mixture are injected into the driver side required to rupture the Al diaphragm. When the diaphragm bursts, the experiment then begins. From Figure 1, at t1 initially a shock wave forms at a short distance away from the diaphragm. The shock wave to the test section is region one where the test mixture resides. Behind the shock wave to the contact surface following the shock wave is known as region 2 which is also traveling down the driven side. Also, a series expansion waves are formed traveling in the opposite direction of the shock wave and contact surface. Between the expansion waves and contact surface is known as region 3 while the expansion waves to driver wall is region 4 where the inert gases preside. As the shock wave propagates through the driven side it compresses the test mixture into the test region. The compression of the test mixture increases the mixture's temperature and pressure then the shock wave reflecting of the test mixture also increases the temperature and pressure to T_5 and P_5 which are ideally the needed test conditions. From the reflected shock wave to the mixtures self-ignition is the Ignition delay time. The shock tubes test time ends when the contact surface (bulk flow of inert gases) collides with the reflected shock or if the expansion waves reach test region (region 5).

For collecting IDTs during experiments, piezoelectric pressure transducers are utilized to gather pressure traces. Six equidistantly spaced pressure transducers are attached to Agilent 53220A time interval counters on the driven side. These are triggered when the incident shock arrives, and the time difference from the six-spaced pressure transducers is used to calculate the shock velocity The uncertainty of 20% of IDTs is affected by the shock velocity measured by timer counters, which, in turn, is influenced by temperature. [25].

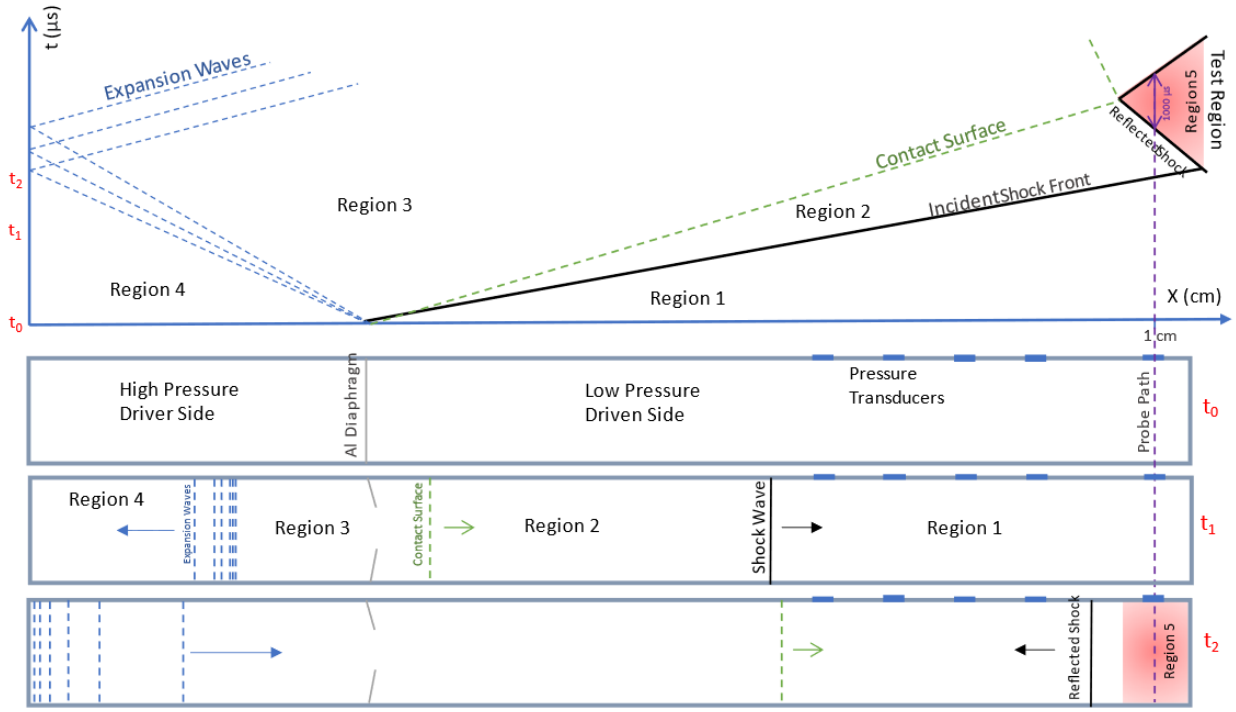

Figure 1: x-t diagram of a Shocktube

Mixture Composition

All tested mixtures were blended in air, which was synthetically produced in-house using ultra-high purity oxygen (O_2) and ultra-high purity nitrogen (N_2), supplied by Nextair and are 99.999% pure. Simulations with different mechanisms to predict ignition delay times were produced using Catera [29]

and Chemkin-Pro [30]. The sensitivity analysis mentioned earlier used Chemkin Pro to identify discrepancies between experimental data and the mechanism. For both softwares (Chemkin and Cantera), IDT simulations are performed using a closed 0-D homogenous batch reactor using a constraint volume problem type. The undiluted mixtures used in the study are presented in Table 3 Based on previous literature, the 60% DME and 40% propane (61.1:38.9% by mass) mixture ratio used, where ideal combustion was found at propane content lower than 40% mass % in CI engines [14]. A few of the experiments were also performed at pressures of 90-120 bar at a temperature range of 900-1100 K for mixtures of 50% DME and 50% propane (fuel mole fraction) at ϕ=0.38.

Table 3: Mixture composition and conditions tested.

Mixture #	Mixture	ϕ	C_3H_8	CH_3OCH_3	O_2	N_2	P_5 (bar)
1	Neat Propane	1	4.03	0	20.16	75.81	60,80
2	Neat DME		0	6.54	19.63	73.82	
3	60/40-DME/Propane		2.10	3.14	19.91	74.85	
4	50/50 – DME/Propane	0.38	1.00	1.00	20.58	77.42	90, 120

Defining Experimental IDTs

The IDTs defined earlier for Shocktubes are captured using an OH* (306 nm) and CH* (432 nm) radical chemiluminescent emission detector via window ports at the test location. IDT calculations can vary from test groups, but having consistency with other works and simulations is essential in determining the definition of an IDT to maintain consistency. For example, IDTs for these experiments were calculated from the experimental time-zero, when the core of the reflected shock passes by the

test section, to when OH* attains a peak value (τ in Figure 2) [31]. Figure 2 shows the experimental pressure, OH* and CH* emissions and pressure traces at the oxidation of DME-propane mixtures. From these figures, we can observe an initial rise in pressure just before the ignition. The increase in pressure is attributed to one of DMEs inert characteristics of dual ignition.

The Shocktube experiments apply the assumption of homogeneous distributed quiescent gas behind the reflected shock under the order of a few milliseconds. This short time frame allows experimental data to be compared to simulated data under constant internal energy and volume assumptions. The adiabatic assumption of the simulations is also satisfied because the heat loss process is negligible because of the microsecond time scale at which the experimentation occurs[12]. The chemical kinetic mechanisms used in this work are Aramco3.0 [31], NUIG [32], and Dames et al. [8]. Most of the analysis in this work was carried out with the Dames et al. [8] model, as it is well-validated for DME-propane mixtures for pressures up to 20 bar.

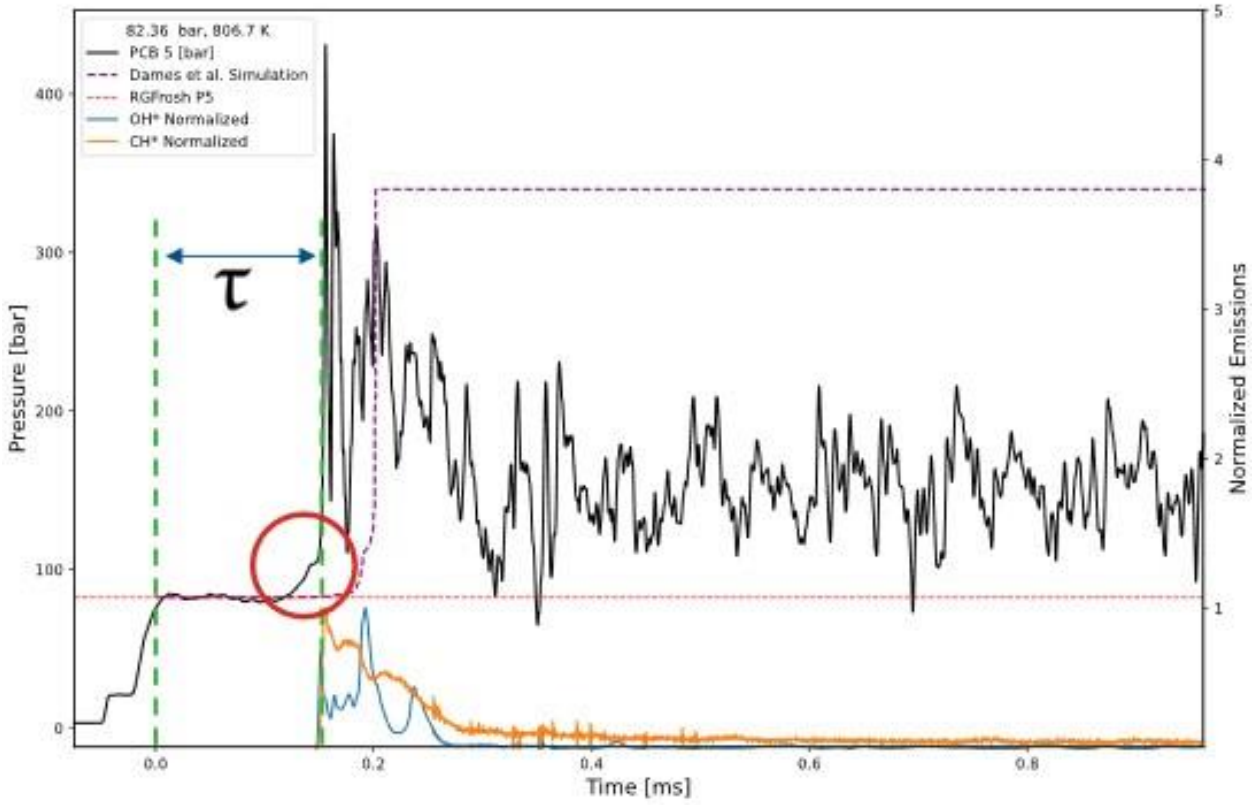

Figure 2: Pictoral shows state 5 pressure conditions prior to ignition onset demonstrating the pressure profile. Example experimental trace showing an increase in the pressure before ignition at the red circle. The conditions shown are for 82.36 bar and 806.7 K for neat DME. Dashed lines show simulated pressure traces obtained using the Dames et al. [8] mechanism.

At lower temperatures as seen from Figure 2 shows a rise in pressure before the main event. This has been attributed to DME dual ignition or two step ignition which is a characteristic of hydrocarbons where low temperature heat release (LTHR) can be observed. The first stage reactions that contribute to LTHR have been studied theoretically by Wada et al. [33]. They observed reactions summarized in Table 4 a prominent reaction in DME oxidation is DME reacting with OH (R7), which occurs after a chain of reactions in the first stage of DME decomposition. DME undergoes H-abstraction with O_2 to produce a radical and HO_2 (R1). The radical proceeds to react with O_2 to form RO_2 (R2), which undergoes isomerization to form QOOH (R3). Following this, it then reacts with O_2 to form OOQOOH (R4). OOQOOH then decomposes to form HPMF + OH (R5). HPMF then decomposes to form another OH

and $OCHOCH_2O$ (R6). Since one DME produces two OH radicals (R4 and R5), it is considered chain branching. These reactions then dominated at lower temperatures, in return they contributed to the increase of pressure before ignition.

Table 4: First Stage Reactions of DME

Reaction	Reaction Reference
$DME+O_2=R+HO_2$	R1
$R+O_2=RO_2$	R2
$RO_2 = QOOH$	R3
$QOOH+O_2=OOQOOH$	R4
$OOQOOH = HPMF + OH$	R5
$HPMF = OH + OCHOCH_2O$	R6

CHAPTER FOUR: RESULTS AND DISCUSSION

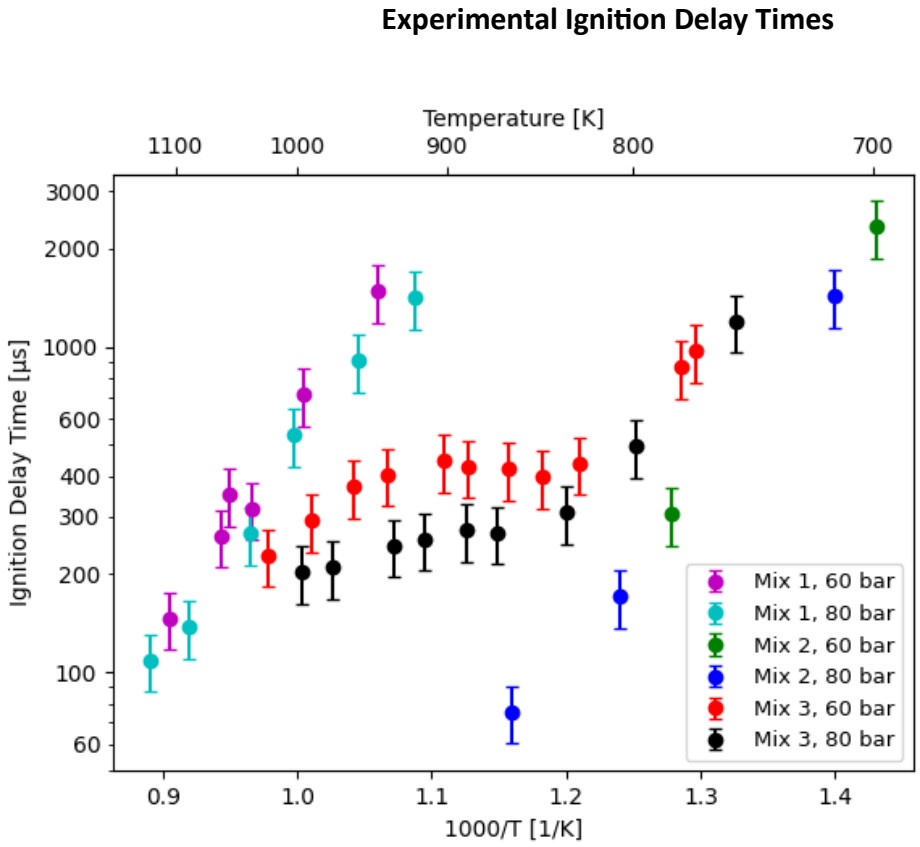

Figure 3: Experimental ignition delay times for various DME mixtures studied in this work at 60 bar and 80 bar at an equivalence ratio of 1.

Figure 3 displays the ignition delay times observed for various mixtures at approximately 60 and 80 bar in this work. The experiments reveal that the neat propane mixture ignites the slowest, while the neat DME mixture ignites the fastest. The neat propane ignition delay times show little pressure dependency, whereas, for the 100% propane mixture, ignition becomes more rapid with increasing pressure. The experiments do not show significant pressure dependency for neat DME at the conditions studied. For the 60/40 blend of DME in the propane mixture, ignition delay times were observed to be faster and slower than in the neat propane mixture. At 60 bar, the ignition delay time decreases as the temperature increases until it reaches 827 K. Beyond 827 K. However, the ignition delay time increases

until it reaches about 900 K, after which the IDT reduces again. This negative temperature coefficient (NTC) behavior for IDT has been observed for DME mixtures in Dames et al.[8]. For 80 bar, the NTC behavior is not as significant as it is for lower pressures (60 bar), although it still exists. The NTC regions could not be experimentally reached for the 100% DME and C_3H_8 mixtures. For DME, instantaneous ignition occurred at higher temperatures, whereas for propane, remote ignition occurred at lower temperatures. As mentioned earlier, DME and propane complement each other very well, allowing for a broad temperature range between 754 – 1022 K at 60 and 80 bar, a much more comprehensive range for testing than the neat mixtures.

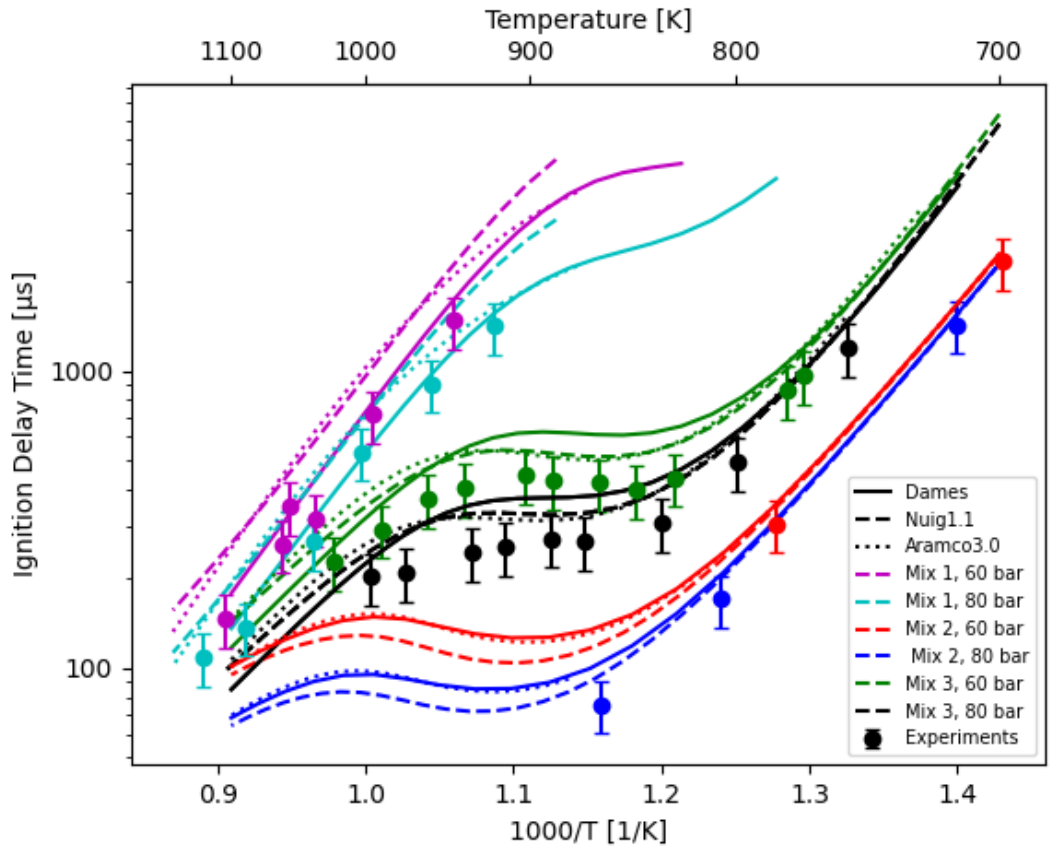

Figure 4: Comparison of experiments and model predictions (NUIG [32] and Dames et al. [8] mechanisms) for ignition delay times of DME-propane mixtures at 60 and 80 bar at an equivalence ratio of 1.

Figure 4 compares the experimental IDTs with the predictions made by three models (NUIG [32], Dames et al. [8], and Aramco3.0 [31]). Overall, all three models show the trend in IDTs for all DME-propane mixtures. For a 100% DME blend, the IDTs predictions are within the experimental uncertainty at both 60 and 80 bar at lower temperatures. The model predictions at 60 and 80 bar converge at lower temperatures for neat DME mixtures, indicating significantly lower pressure dependency, which is in line with our experimental observations. However, as temperature increases, the models diverge, displaying higher pressure dependency at high temperatures. All three mechanisms accurately predicted low-temperature IDTs for neat DME. As temperature increases, deviations are observed, with experimental IDTs being faster than predicted values.

The Dames et al. [8]. mechanism is more accurate than the NUIG [32] and Aramco3.0 mechanism in predicting the experimental IDTs for neat propane at 60 and 80 bar. However, for the 60/40 blend of DME-propane, all mechanisms overpredict the IDTs. The NUIG [32] and Aramco3.0 [31] models are closer to experiments at lower temperatures. Even after blending with 40% propane, the trend of decreasing pressure dependency when lowering the temperature is still retained, similar to a neat DME mixture. At higher temperatures, the most accurate model is the Dames et al. [8]. The NTC behavior for the 80 bar experiments is different from that of 60 bar. Instead of a significant rise before falling, the trend is flatter and quickly trends downward at approximately 950K. The NUIG [32] mechanism is the most accurate at lower temperatures before the NTC region, where the values are within the experimental uncertainty. In the NTC region, the most accurate mechanism is Aramco3.0 [31]. However, at higher temperatures near the end of the NTC region, the experimental data has a much smaller slope when compared to the predictions of mechanisms where they curve out and then plateau. In this region, the most accurate mechanism is the model of Dames et al. [8].

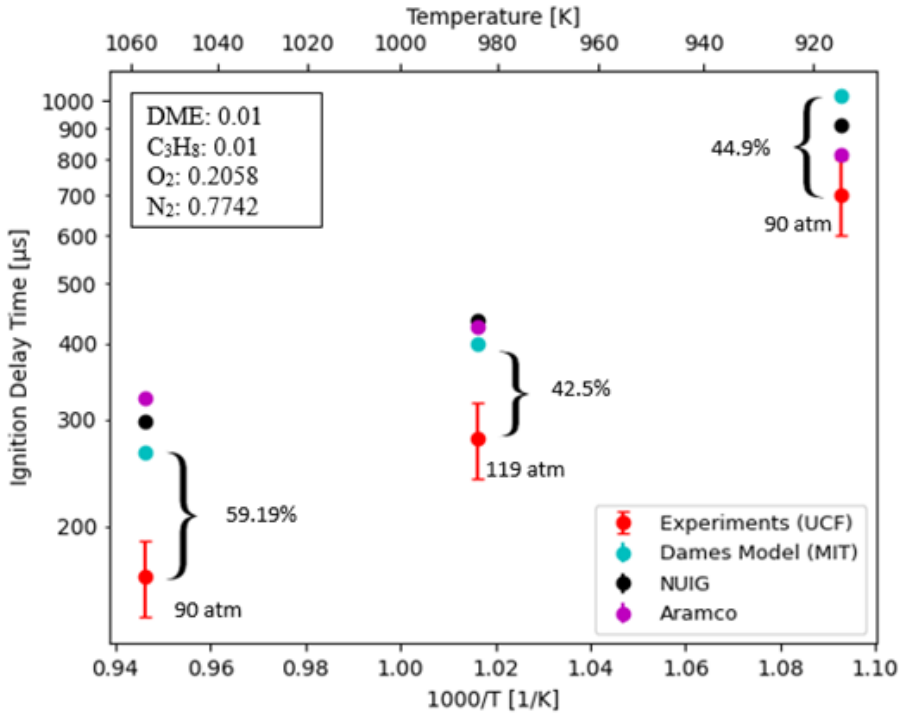

Figure 5: Experimental results obtained for IDTs compared with simulation results for DME-propane mixture at ~90 and ~120 bar. See text for mechanisms.

In Figure 5, the ignition delay times (IDTs) obtained from experiments conducted at 90 and 120 bar are shown along with the predicted IDTs obtained from reaction mechanisms from the literature. The experimental results show that the IDTs are much faster than the predicted ones, and the deviations from the models are more significant as the pressure increases. The Aramco3.0 [31] mechanism predicts the slowest ignition at higher temperatures, and its accuracy improves as temperatures decrease. On the other hand, the Dames et al. [8] mechanism predicts the fastest ignition at two points. The NUIG [32] mechanism is in between Aramco3.0 [31] and Dames et al. model [8] for two points. For 119 atm, Aramco and NUIG [32] predict similar IDTs, but the Dames et al. [8] model has the best prediction. The Dames et al. [8] model has the closest prediction to the experimental results regarding deviation from the model. The model shows a deviation of around 59% with the experimental results at high

temperatures and around 44.9% at lower temperatures. This indicates that the current models available in the literature for DME/propane blend need to be revised to model high-pressure ignition scenarios accurately, which are typical in heavy-duty engines.

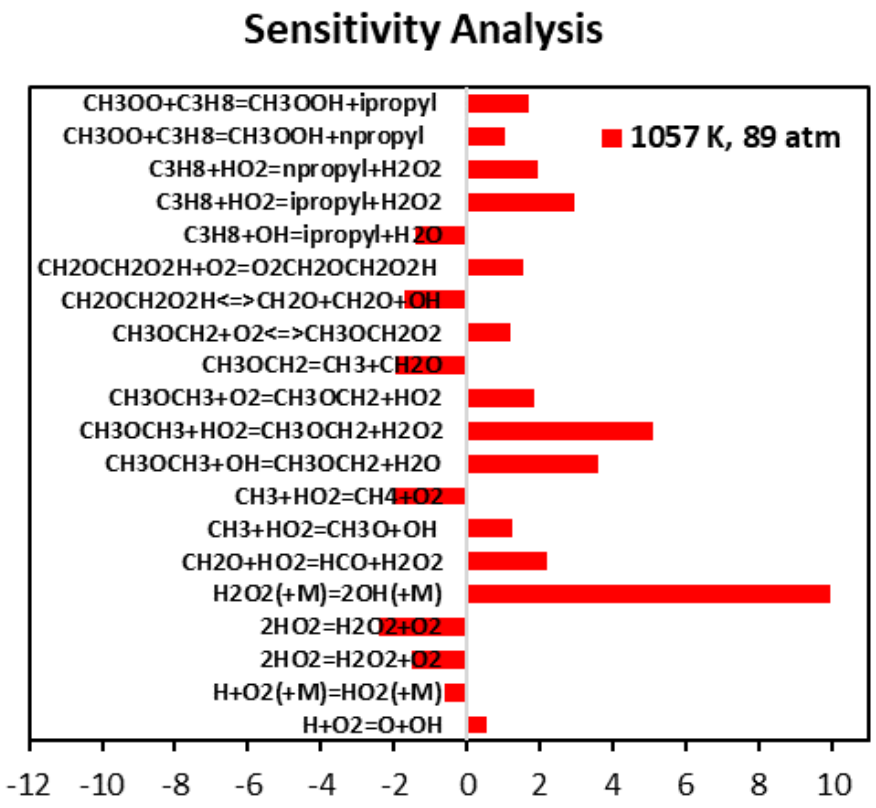

Figure 6: Sensitivity analysis using the Dames et al. [8] mechanism at the time when half of the DME in the mixture is consumed (1057 K and 89 atm).

A sensitivity analysis was conducted using the Dames et al. [8] model to understand the discrepancies between the model and experiments. The sensitivity analysis was carried out for the high-temperature scenario (1057 K and 89 atm), which exhibited the most significant deviation from experimental results. Figure 6 shows the outcomes for the top 20 reactions when 50% of DME was consumed. The most sensitive reaction was H_2O_2 (+M) = 2OH (+M). This reaction is well-researched, and the rate is well established. The second most sensitive reaction was $CH_3OCH_3 + HO_2 = CH_3OCH_2 + H_2O_2$,

which is the H-abstraction from DME by HO_2 radical. This is due to the mixture being investigated containing 50% propane in the fuel, and propane undergoes H-abstraction at high temperatures to produce the C_3H_7 radical. The C_3H_7 radical produced then reacts with oxygen to produce HO_2 radicals. The higher amount of HO_2 in the reaction pool makes this H-abstraction by HO_2 one of the most sensitive reactions for the DME/propane mixture. The rate constant for this reaction is from the theoretical work by Mendes et al. [34] and has an estimated uncertainty of a factor of 2.5. Other sensitive reactions include H-abstraction by OH and O_2. These rates were estimated by Curran and Fisher [35] and are prone to significant uncertainties [35]. The IDT for this mixture is also sensitive to a few pressure-dependent reactions of DME intermediates like $CH_2OCH_2O_2H + O_2 = O_2CH_2OCH_2O_2H$ and $CH_3OCH_2 + O_2 = CH_3OCH_2O_2$. Both rates are from Burke et al. [36], which made several assumptions to derive these rates using theoretical calculations from Yamada et al.[37] and the high-pressure rate from Li et al. [38].

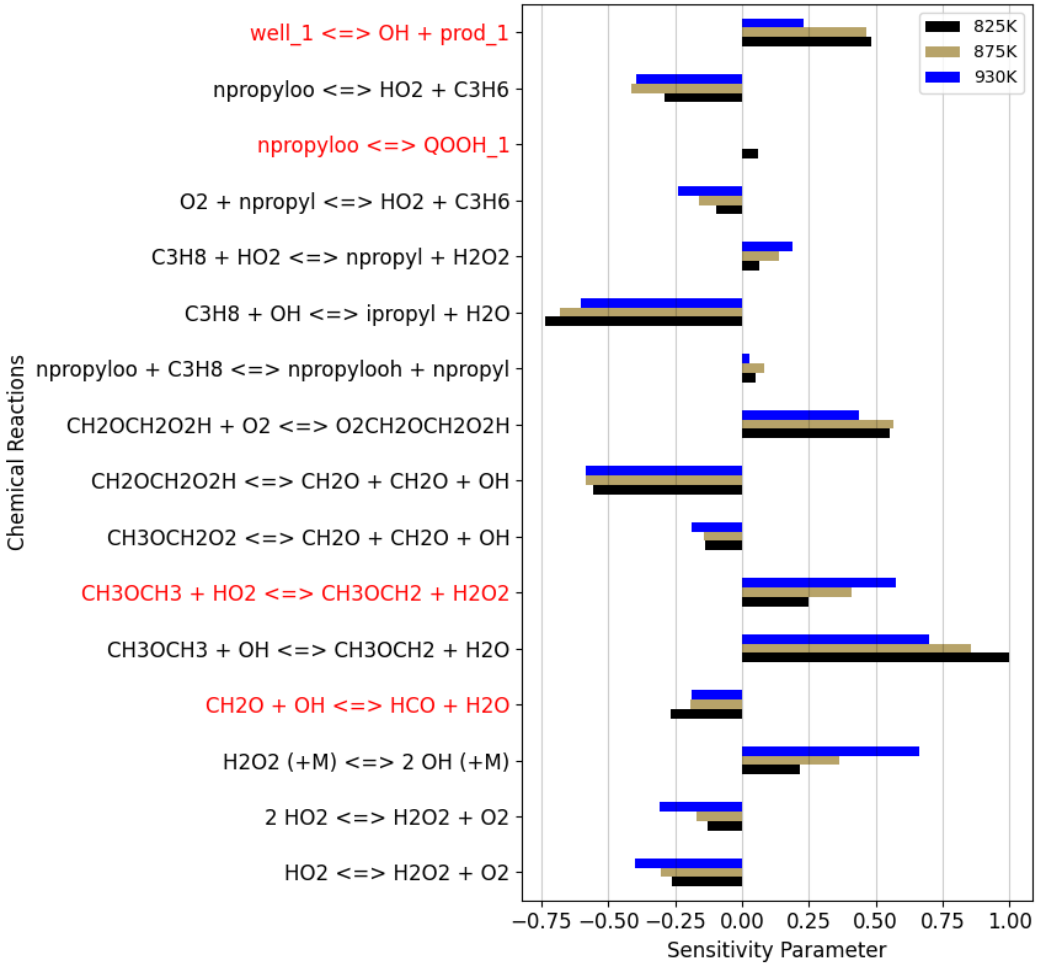

Figure 7: Sensitivity analysis of 60 bar Mix 3 conducted with Dames at al [8]at 50% fuel consumption at temperature of 825, 875, and 930 K

In order to investigate the NTC region and the deviation from the NTC estimated from the Dames et al model [8] from mix 3. Another sensitivity analysis was conducted as shown in Figure 7. From the sensitivity analysis we can notice the most prominent propagating reaction is an initial reaction with $CH_3OCH_3 + OH = CH_3OCH_2 + H_2O$ while the most terminating reaction is $C_3H_8 + OH$ =ipropyl + H_2O. From the sensitivity analysis, the initial reaction $CH_3OCH_3 + HO_2 = CH_3OCH_2 + H_2O_2$ was modified as it was the most sensitive at 930 K the peak of the NTC region and where the model deviated the greatest. Following the modification three other modifications were made to the reactions highlighted in red in

Figure 7. The reactions modified are available in Table 5. The second reaction modified was reaction 678, well_1 = OH prod_1 which had an uncertainty facto of 2 [39] where Goldsmith et al. had done theoretical work for reactions of O_2 with hydroperoxyl alkyl radicals. Reaction 678 was modified by a factor of 2. Following this, reaction 53, CH_2O + OH <=> HCO + H_2O which is an H-abstraction from formaldehyde to produce HCO and water was reduced by a factor of 2. Reaction 53 was experimental work done with chemical kinetic data for chemistry for methane and related compounds done by Tsang et al [40]. The final reaction modified was reaction 636 which was an isomerization of npropyloo = QOOH_1. Reaction 636 has an uncertainty of 2 and was modified by a factor of 2 by Goldsmith et al. [39].

The new modified mechanism was then compared to the experimental data in Figure 8, Figure 9. As the modifications were made to target the NTC region, the mechanism ability to predict DME/propane chemistry at the NTC region has greatly improved. But the modified model is now also within the uncertainty before and after the NTC region at higher temperatures for mix 3. For Mix 1 the model for 60 is more in line with trend of experimental data points while 80 bar the model had slight deviations within the experimental uncertainty. For neat DME, at higher temperatures the model is now within uncertainty of the experiments. The same model was then used for the preliminary data gathered for mix 4. For all three experiments the modified model has shown improvement in the prediction of DME/propane chemistry.

Table 5: Reactions modified for the Dames et al. mechanism using the sensitivity analysis shown in Figure 6

Reaction Number	Reactions Changed	A Factor
356	$CH_3OCH_3 + HO_2 <=> CH_3OCH_2 + H_2O_2$	*1.5
678	well_1 <=> OH + prod_1	*2
53	$CH_2O + OH <=> HCO + H_2O$	*0.5
636	npropyloo <=> QOOH_1	*2

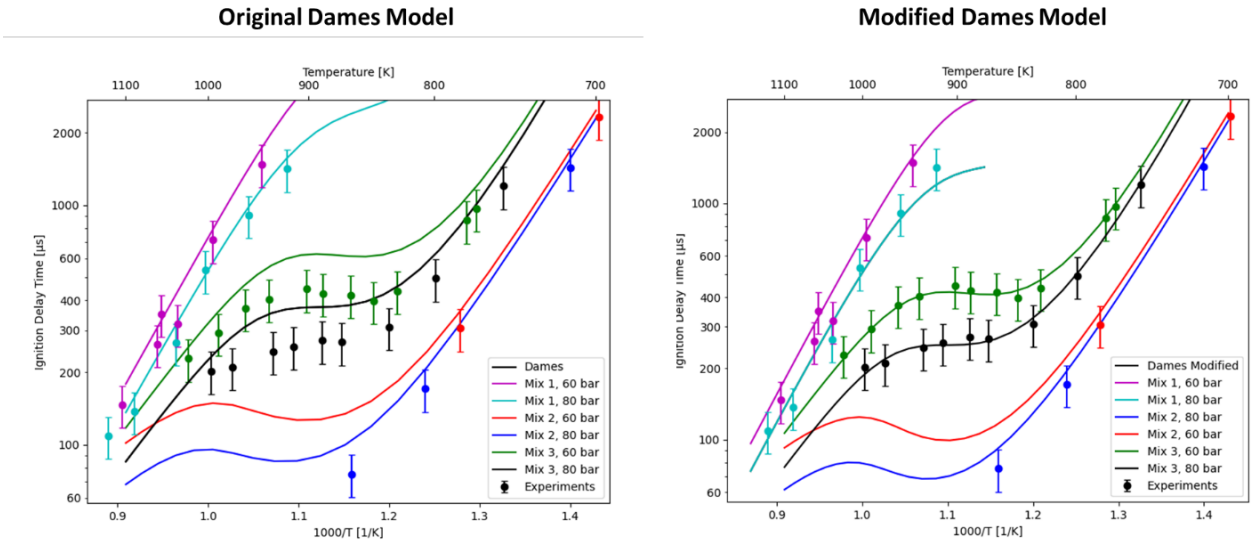

Figure 8: Comparison of experimental results with the predictions by the Dames et al. [8] model and the modified version of the Dames et al. [8] model for IDTs of DME-propane mixtures (60 and 80 bar) at an equivalence ratio of 1.

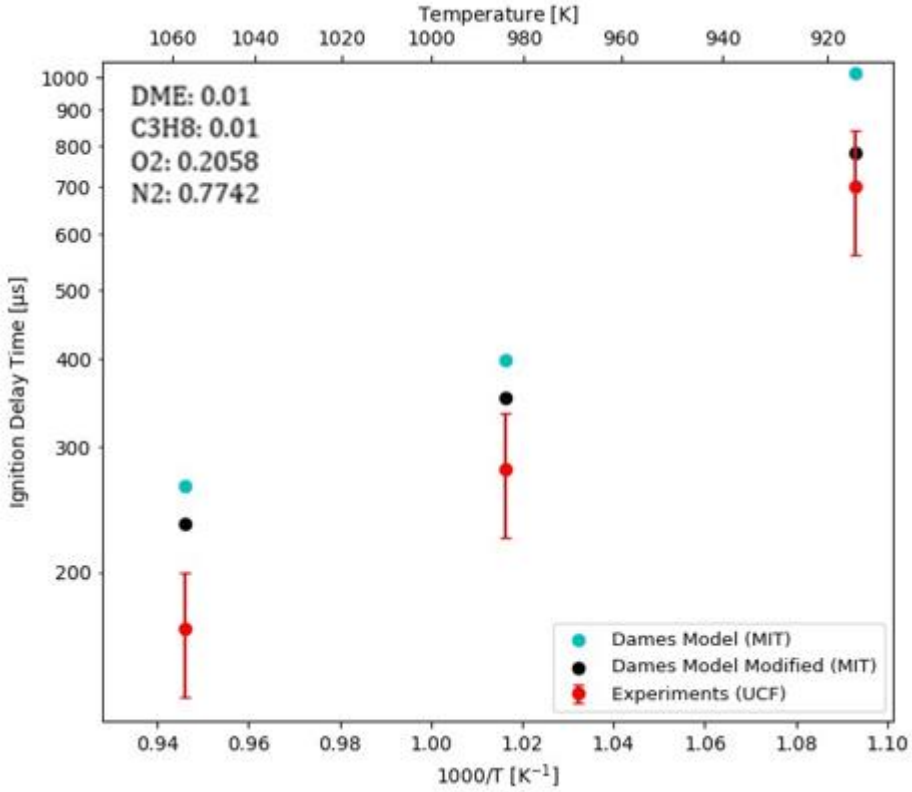

Figure 9: Comparison of experimental results with the predictions of the Dames et al. [8] mechanism and the modified version for IDTs of DME-propane mixtures at 90-120 bar.

Pathway Analysis

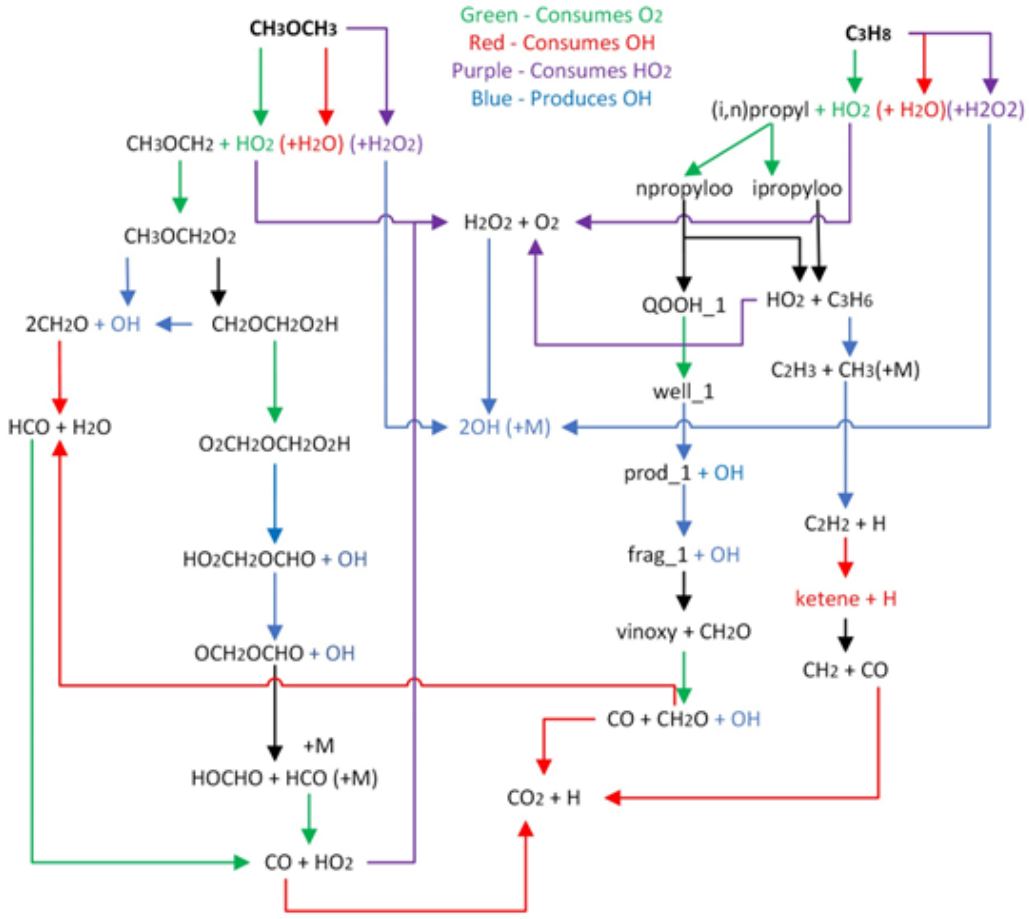

Figure 10: Chemical Reaction Pathway for 900K of DME/C_3H_8 at 60 bar of some of the more prominent reactions

To better explain the chemical kinetics observed at the NTC region of mix 3 (ϕ=1.0) from Figure 8, reaction pathways were analyzed using the Dames et al. [8] mechanism in Chemkin Pro [30]. From Figure 10, The initial reactions observed are the reactions of DME and propane because their reactions with O_2 have the same magnitude of activation energy. DME combustion results in an H-abstraction from DME to oxygen to produce hydroperoxyl (HO_2) and methoxymethyl radicals (CH_3OCH_2) as shown in reaction R358 from, and has an activation energy of 44,910 cal/mol-K. Propane undergoes H-abstraction reaction with oxygen to produce n/i-propyl and HO_2 (R- alkyl radical) with activation energies of 52,290

cal/mol-K and 49,640 cal/mol-K respectively (Reaction R453 & R452 in Table 6), and propyl radicals are very important in the low-temperature combustion of propane. n-R then reacts with another oxygen molecule to form n-RO_2 (R629 and R645 from Table 6), the alkyl peroxyl radical. Hydroperoxyl propyl radicals (QOOH_1), as seen in Figure 10, are from the intermolecular rearrangement of propyl peroxyl radicals (n-RO_2) (R636 from Table 6) [41]. This reaction also occurs during the NTC region at 900 K during the combustion of DME/C_3H_8, but n-RO_2 pyrolysis to HO_2 and propene (C_3H_6) was observed to be more prominent before ignition for lower temperatures (R638).

Table 6: Reaction number and chemical equations reference for prominent reactions in DME and propane

Reaction Label	Reaction
R358	$CH_3OCH_3 + O_2 <=> CH_3OCH_2 + HO_2$
R453	$C_3H_8 + O_2 <=> nR + HO_2$
R452	$C_3H_8 + O_2 <=> iR + HO_2$
R629	$O_2 + nR <=> nRO_2$
R645	$O_2 + iR <=> iRO_2$
R636	n-RO_2 ⇔ QOOH_1
R638	n-RO_2 ⇔ $HO_2 + C_3H_6$

Following the formation of QOOH_1, it produces well_1 (3-hydroperoxyl-n-propylperoxy) by reacting with O_2, as shown in reaction R655 from Table 7. Well_1 is then decomposed at high temperatures to prod_1 (2-formyl-ethyl-hydroperoxide), releasing an OH radical (R678). In any

combustion system, the OH radicals are the most important as they guide the combustion process[42] and are a critical radical for chain propagation reactions. In a DME-propane system, when OH is produced, it will react with DME at a higher rate than propane as the activation energy for OH reacting with DME (780.7 cal/mol-K for R353) is lower than its reaction with propane (2186.5 and -86.8 cal/mol-K for R458 and R459 from Table 7). This is clear from Figure 11, which shows the higher consumption of OH radicals by reaction R353 compared to R458 and R459. The resultant products of DME reacting with OH are CH_3OCH_2 and H_2O, as shown in reaction R353 in Table 7; CH_3OCH_2 then undergoes a reaction with molecular oxygen to form the methoxymethyl peroxyl radical ($CH_3OCH_2O_2$) (R364). $CH_3OCH_2O_2$ then rearranges to form $CH_2OCH_2O_2H$ (R367), or instead, $CH_3OCH_2O_2$ decomposes to form two molecules of formaldehyde (CH_2O) and OH radical (R368). $CH_2OCH_2O_2H$ then reacts with O_2 to form $O_2CH_2OCH_2O_2H$ (R370), which decomposes to form HO_2CH_2OCHO and OH (R372). Further following this reaction pathway, HO_2CH_2OCHO decomposes to OCH_2OCHO and OH (R373), which occurs due to the high temperatures. with the product (OCH_2OCHO) decomposing further: OCH_2OCHO (+M) = HOCHO + HCO (+M) (R374). The OH formed during all of the above reactions will react swiftly with unreacted DME in the reaction pool, as reaction R353 is very fast due to its low activation energy, as discussed before. OH is also consumed for the reaction with formaldehyde (CH_2O) to produce HCO and H_2O (R53). HCO will then react with O_2 to form important end products of CO and H_2O (R40). The carbon monoxide then reacts with OH radicals to produce carbon dioxide and an H radical (R32). As discussed, during the oxidation of DME, OH radicals serve as strong initiators in the NTC regime as more is produced than consumed.

Table 7: Continuation of Table 6, reaction number and chemical equations reference for prominent reactions in DME and propane

Reaction Index	Reaction
R655	O_2 + QOOH_1 ⇔ well_1
R678	Well_1 ⇔ OH + prod_1
R353	CH_3OCH_3 + OH ⇔ CH_3OCH_2 + H_2O
R458	C_3H_8 + OH <=> npropyl + H_2O
R459	C_3H_8 + OH <=> ipropyl + H_2O
R364	CH_3OCH_2 + O_2 ⇔ $CH_3OCH_2O_2$
R367	$CH_3OCH_2O_2$ ⇔ $CH_2OCH_2O_2H$
R368	$CH_3OCH_2O_2$ ⇔2CH_2O + OH
R370	$CH_2OCH_2O_2H$ + O_2 ⇔ $O_2CH_2OCH_2O_2H$
R372	$O_2CH_2OCH_2O_2H$ ⇔ HO_2CH_2OCHO + OH
R373	HO_2CH_2OCHO ⇔ OCH_2OCHO + OH
R374	OCH_2OCHO(+M) = HOCHO + HCO (+M)
R53	CH_2O + OH⇔HCO + H_2O
R40	HCO + O_2 ⇔ CO + HO_2
R32	CO + OH ⇔ CO_2 + H

The HO_2 radicals produced from DME decomposition react with DME and propane. These reactions are DME reacting which results in a H-abstraction from DME to HO_2 forming H_2O_2 (R356). C_3H_8 reacting with HO_2 produces (n,i)R and H_2O_2 (R461,and R460). Hydrogen peroxide (H_2O_2) is another important radical produced from two hydroperoxyl radicals $2HO_2$ reacting to produce H_2O_2 and O_2 (R22) . The H_2O_2 radicals are important to the combustion of C_3H_8 and DME as they form 2OH (+M) through decomposition (R24). iR produced from propane is also a product of propane reacting with HO_2 (R461) which then reacts with O_2 (R453) to produce i-RO_2. Then through a unimolecular reaction, iR decomposes to HO_2 + C_3H_6. nR also shares this pathway for a wide variety of temperatures lower and higher than 900K. However, the two reactions nRO_2 = QOOH_1 and nRO_2 = HO_2 + C_3H_6 are competing. Outside of the NTC region at higher temperatures, nRO_2 = QOOH_1 is more prominent but during the peak of the NTC (900K), the reaction nRO_2 = HO_2 + C_3H_6 overtakes for a prolonged time as seen from Figure 13. For 900 K, nRO_2 = HO_2 + C_3H_6 is observed to be more prominent but when production for QOOH rises, the production of propene and HO_2 decreases and reaction nRO_2 = QOOH_1 becomes more prominent, and ignition occurs. Following propene, it then decomposes to ethylene (C_2H_3) and the methyl radical (CH_3) (R491). Following the product C_2H_3, decomposes into acetylene (C_2H_2) and a H. Further, C_2H_2 reacts with an OH radical to produce ketene and hydrogen (R273). Then carbon monoxide is detached from ketene through bond cleavage for products of CH_2 and CO (R132).

Table 8: Continuation of table 6 and 7 labeling reactions

Reaction Index	Reaction
R356	$CH_3OCH_3 + HO_2 <=> CH_3OCH_2 + H_2O_2$
R461	$C_3H_8 + HO_2 <=> nR + H_2O_2$
R460	$C_3H_8 + OH <=> iR + H_2O_2$
R22	$2HO_2 <=> H_2O_2 + O_2$
R24	H_2O_2 (+M) ⇔ 2OH (+M)
R491	$C_2H_3 + CH_3$ (+M) ⇔ C_3H_6 (+M)
R263	C_2H_2 + H (+M) ⇔ C_2H_3 (+M)
R273	$C2H_2$ + OH ⇔ketene + H
R132	CH_2 + CO (+M) ⇔ketene(+M)

Figure 12, references the evolution of some important radicals present from Figure 10. During ignition, however, OH increases rapidly and H_2O_2 and H_2O are consumed. When H_2O_2 is consumed it produces two OH radicals which does play a role in the production of OH during ignition during 500 – 630 microseconds. The production of OH is lower than the other radicals because it is constantly reacting with other species at a higher rate, especially before ignition around 300 – 550 us where it is almost stagnant.

Table 9: Reaction index and chemical equations reference for prominent reactions in DME and propane

Reaction Index	Reaction
353	$CH_3OCH3 + OH <=> CH_3OCH_2 + H_2O$
458	$C_3H_8 + OH <=> nR + H_2O$
459	$C_3H_8 + OH <=> iR + H_2O$
636	$nRO_2 <=> QOOH\_1$
638	$nRO_2 <=> HO_2 + C_3H_6$

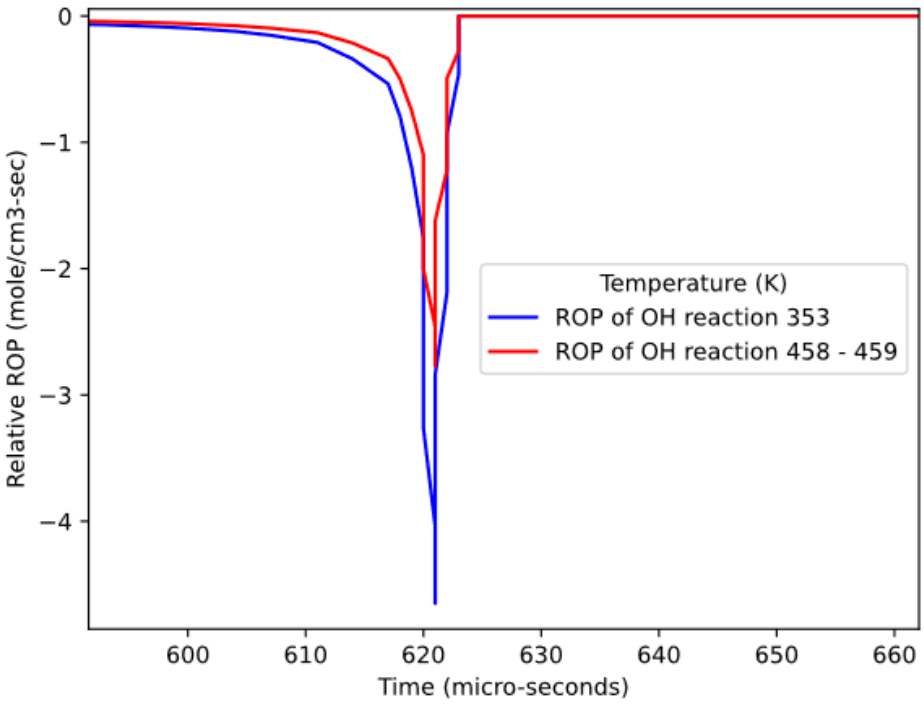

Figure 11: ROP of OH from DME and Propane reactions. Graph representing the rate of production of two chemical equations using Dames et al. [8]

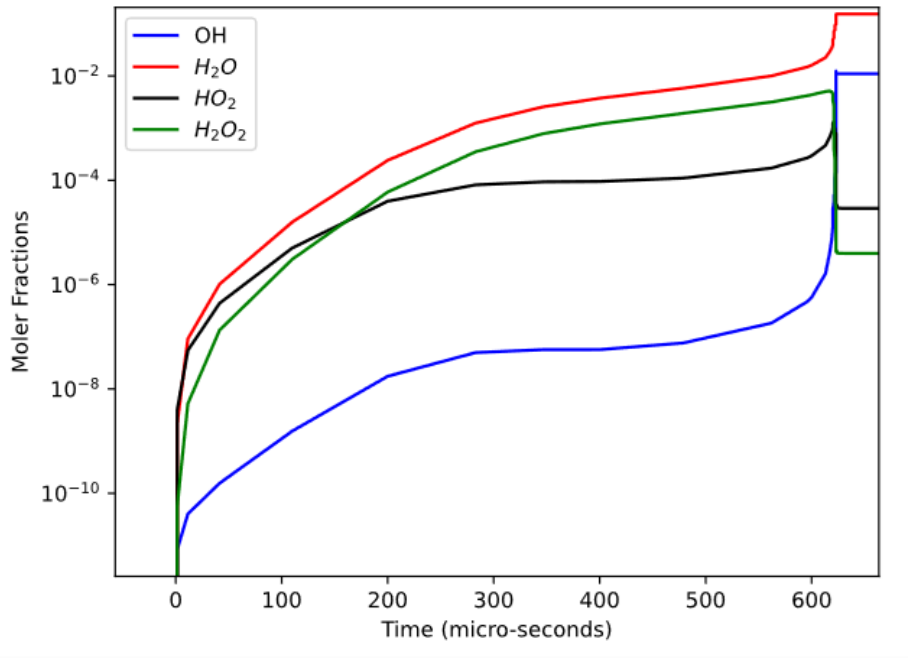

Figure 12: Mole fractions of radicals for 900K of a DME/propane blend.

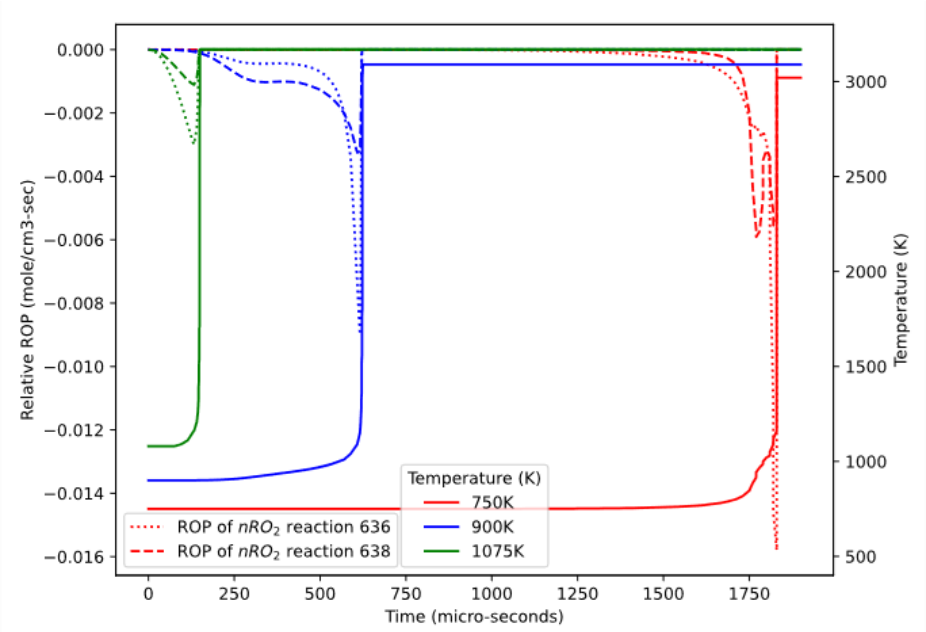

Figure 13: The solid line is the temperature (K) while the dashed line is the ROP of OH from both initial propane reactions and the dotted is from DME + OH using Dames et al. [8]

Figure 13 depicts the ROP of nRO_2 for reactions 636 and 638 for three different temperatures at 60 bar. By observing the ROP for the two lower temperatures, reaction 636 consumes more nRO_2 than reaction 636 at 1750 to 1800 µs for 750 K, and 150 to 560 µs for 900 K. After the first intersection of the two ROP values, 560 µs for 900 K and 1750 µs for 750 K, it is observed from Figure 13 that temperature starts to incline till reaction 636 overtakes reaction 638 where ignition occurs. If consumption of nRO_2 leans towards reaction 638, it will inhibit/delay ignition. As we increase in temperature, the role of reaction 638 decreases to 1075 K where reaction 636 remains dominant through ignition at 150 µs. By modifying reaction 638, multiplying the A-factor by *2 it is apparent that the NTC region shifts upwards. By increasing the A-factor the reaction is more prominent in ignition and a NTC region shifting upwards indicates that this reaction inhibited ignition. This was a conclusion drawn from Figure 13 and by decreasing the A-factor of reaction 638, an opposite effect of a decreased ignition delay at the NTC region could be observed.

CHAPTER FIVE: CONCLUSION

IDTs for mixtures of DME-propane were measured for conditions relevant to mixing controlled compression ignition engines (60-120 bar and 700-1100 K). Undiluted experiments, spanning temperatures of 700 to 1100 K and pressures near 60 and 80 bar for various blends (100% CH_3OCH_3, 100% C_3H_8, 60% CH_3OCH_3 | 40% C_3H_8) of DME and propane were combusted in synthetic air (21% O_2 | 79% N_2). In order to understand the effect of higher pressures, some experiments were conducted near 90 and 120 atm. NTC behavior was observed with a 60/40 blend of DME with propane. At higher pressures (80 bar), NTC was less prominent than at lower pressures (60 bar). Against the experimental IDT data, comparisons are made with predictions of recent chemical kinetic mechanisms for the DME-propane mixture, including the Aramco3.0 [31], NUIG [32], and Dames et al. [8] mechanisms. Models were able to capture the general trend in experimental IDTs for 60 and 80 bar cases. However, when compared to experimental results, none of the models could fully predict the behavior across the entire region of interest. For 90 and 120 bar cases, significant deviations from experiments were observed for model predictions. All mechanisms overpredict IDTs compared to experimental values. Sensitivity analysis was conducted with the Dames et al. [8] mechanism, and critical reactions sensitive to IDT of DME-propane mixture at 60 bar were outlined. Future work will involve collecting data for additional mixtures and experimental conditions (pressure, temperature) as well as probing intermediates and products using laser absorption techniques during the ignition process for additional insights into this promising fuel blend chemistry. From observing the chemical kinetics of the NTC region it is observed that reaction 638 inhibits ignition while reaction 636 promotes ignition for propane.

APPENDIX: MIXTURE AND IDT INFORMATION

Table 10: Summary of neat DME mixture data ($C_2H_6O/O_2/N_2$ = 6.6/19.6/73.8)

T_5 (K)	P_5 (atm)	*IDT* (μs)
699	60	2334
782	58	306
714	86	1431
807	82	171
863	84	75
915	84	59

Table 11: Summary of neat C_3H_8 mixture data ($C_3H_8/O_2/N_2$ = 4/20.2/75.8)

T_5 (K)	P_5 (atm)	*IDT* (μs)
944	60	1480
995	60	714
1035	62	319
1054	64	351
1059	62	262
1105	61	147
920	79	1415
957	79	907
1003	82	534
1036	80	266
1089	83	137.5
1124	84	108.9

Table 12: Summary of neat C_3H_8/DME blend data ($C_3H_8/CH_3OCH_3/O_2/N_2$ = 2.1/3.14/19.91/74.85)

T_5 (K)	P_5 (atm)	*IDT* (μs)
771	60	967
778	55	864
827	61	438
846	60	398
864	59	421
887	59	428
902	57	447
937	59	405
960	59	371
989	59	293
1022	58	229
754	82	1200
799	81	493
833	80	309
871	80	268
888	77	272
914	79	257
933	78	245
974	80	210
997	80	203

Table 13: Summary of experimental IDTs for DME/C_3H_8 (DME/C_3H_8/O_2/N_2= 1/1/20.58/77.42)

T_5 (K)	P_5 (atm)	*IDT* (μs)
984	119	280
1057	89	166
915	87	701

LIST OF REFERENCES

[1] E.-E. I. Administration, "Annual Energy Outlook 2023," 2020. [Online]. Available: https://www.eia.gov/outlooks/aeo/pdf/AEO2023_Narrative.pdf.

[2] IEA. https://www.iea.org/reports/co2-emissions-in-2022 (accessed.

[3] C. Bae and J. Kim, "Alternative fuels for internal combustion engines," *Proceedings of the Combustion Institute,* vol. 36, no. 3, pp. 3389-3413, 2017.

[4] J. Baker, R. Khaleel Rahman, E. M. Ninnemann, and S. Vasu, "Ammonia Hydrogen Ignition Measurements for Clean Aircraft Propulsion," in *AIAA SCITECH 2022 Forum*, 2022, p. 0817.

[5] S. H. Park and C. S. Lee, "Applicability of dimethyl ether (DME) in a compression ignition engine as an alternative fuel," *Energy Conversion and Management,* vol. 86, pp. 848-863, 2014.

[6] H. Stichnothe and A. Azapagic, "Bioethanol from waste: Life cycle estimation of the greenhouse gas saving potential," *Resources, Conservation and Recycling,* vol. 53, no. 11, pp. 624-630, 2009.

[7] E. ToolBox, "Fuels and Chemicals—Autoignition Temperatures," ed, 2003.

[8] E. E. Dames, A. S. Rosen, B. W. Weber, C. W. Gao, C.-J. Sung, and W. H. Green, "A detailed combined experimental and theoretical study on dimethyl ether/propane blended oxidation," *Combustion and Flame,* vol. 168, pp. 310-330, 2016.

[9] M. Matzen and Y. Demirel, "Methanol and dimethyl ether from renewable hydrogen and carbon dioxide: Alternative fuels production and life-cycle assessment," *Journal of cleaner production,* vol. 139, pp. 1068-1077, 2016.

[10] M. Semmel, R. E. Ali, M. Ouda, A. Schaadt, J. Sauer, and C. Hebling, "Power-to-DME: A cornerstone towards a sustainable energy system," in *Power to Fuel*: Elsevier, 2021, pp. 123-151.

[11] S. L. Kokjohn, "Reactivity controlled compression ignition (RCCI) combustion," The University of Wisconsin-Madison, 2012.

[12] E. Ninnemann *et al.*, "New insights into the shock tube ignition of H2/O2 at low to moderate temperatures using high-speed end-wall imaging," *Combustion and Flame,* vol. 187, pp. 11-21, 2018.

[13] G. Agafonov, V. Smirnov, and P. Vlasov, "A Shock-Tube and Modeling Study of Soot Formation During Pyrolysis of Propane, Propane/Toluene and Rich Propane/Oxygen Mixtures," *Combustion science and technology,* vol. 182, no. 11-12, pp. 1645-1671, 2010.

[14] S. Kajitani, C. Chen, M. Oguma, M. Alam, and K. Rhee, "Direct injection diesel engine operated with propane-DME blended fuel," SAE Technical Paper, 0148-7191, 1998.

[15] Z. P. Mohammed, R. K. Rahman, M. Pierro, J. Urso, and S. Vasu, "DME-Propane Ignition Delay Time Measurements at Mixing Controlled Compression Ignition Engine-Relevant Conditions," SAE Technical Paper, 0148-7191, 2023.

[16] L. Zhu *et al.*, "A wide range experimental study and further development of a kinetic model describing propane oxidation," *Combustion and Flame,* vol. 248, p. 112562, 2023.

[17] L. Xu, L. Ouyang, Z. Geng, H. Li, Z. Huang, and X. Lu, "Experimental and Kinetic Study on Ignition Delay Times of Liquified Petroleum Gas/Dimethyl Ether Blends in a Shock Tube," *Energy & Fuels,* vol. 28, no. 11, pp. 7168-7177, 2014/11/20 2014, doi: 10.1021/ef5014133.

[18] M. A. Burnett and M. S. Wooldridge, "An experimental investigation of flame and autoignition behavior of propane," *Combustion and Flame,* vol. 224, pp. 24-32, 2021.

[19] R. Lawson, V. Gururajan, A. Movaghar, and F. N. Egolfopoulos, "Autoignition of reacting mixtures at engine-relevant conditions using confined spherically expanding flames," *Proceedings of the Combustion Institute,* vol. 38, no. 2, pp. 2285-2293, 2021.

[20] A. Tereza, P. Kozlov, G. Y. Gerasimov, V. Y. Levashov, I. Zabelinsky, and N. Bykova, "Shock-tube study of high-temperature ignition of propane-air mixtures at elevated pressures," *Acta Astronautica,* vol. 204, pp. 705-710, 2023.

[21] W. Xia *et al.*, "Shock tube and modeling study of ignition delay times of propane under O2/CO2/Ar atmosphere," *Combustion and Flame,* vol. 220, pp. 34-48, 2020.

[22] S. Eckart, S. Benaissa, R. A. Alsulami, K. A. Juhany, H. Krause, and A. Mohammad, "Laminar burning velocity, emissions, and flame structure of dimethyl ether-hydrogen air mixtures," *International Journal of Hydrogen Energy,* 2023.

[23] A. Stagni, S. Schmitt, M. Pelucchi, A. Frassoldati, K. Kohse-Höinghaus, and T. Faravelli, "Dimethyl ether oxidation analyzed in a given flow reactor: Experimental and modeling uncertainties," *Combustion and Flame,* vol. 240, p. 111998, 2022.

[24] K. C. Bavandla, D. Zhou, A. Tripathi, Z. Sun, and S. Yang, "Characterization of the chemical kinetics of dimethyl ether (DME) in a controlled trajectory-rapid compression and expansion machine (CT-RCEM)," *Combustion and Flame,* vol. 253, p. 112819, 2023.

[25] J. J. Urso *et al.*, "Characterization of a new ultra-high pressure shock tube facility for combustion and propulsion studies," *Review of Scientific Instruments,* vol. 93, no. 6, p. 063905, 2022.

[26] M. Pierro *et al.*, "High-Fuel Loading Ignition Delay Time Characterization of Hydrogen/Natural Gas/Ammonia at Gas Turbine-Relevant Conditions Inside a High-Pressure Shock Tube," in *Turbo Expo: Power for Land, Sea, and Air*, 2022, vol. 86007: American Society of Mechanical Engineers, p. V03BT04A002.

[27] *PyRGFROSH: A frozen shock solver for ideal and real gas equations of state*. (2022). [Online]. Available: https://vasulab.github.io/PyRGFROSH

[28] A. G. Gaydon and I. R. Hurle, *The shock tube in high-temperature chemical physics*. Reinhold Publishing Corporation, 1963.

[29] *Cantera: An Object-oriented Software Toolkit for Chemical Kinetics, Thermodynamics, and Transport Processes*. (2022). https://www.cantera.org.

[30] R. J. Kee, F. M. Rupley, and J. A. Miller, "Chemkin-II: A Fortran chemical kinetics package for the analysis of gas-phase chemical kinetics," Sandia National Lab.(SNL-CA), Livermore, CA (United States), 1989.

[31] C.-W. Zhou *et al.*, "An experimental and chemical kinetic modeling study of 1,3-butadiene combustion: Ignition delay time and laminar flame speed measurements," *Combustion and Flame,* vol. 197, pp. 423-438, 2018/11/01/ 2018, doi: https://doi.org/10.1016/j.combustflame.2018.08.006.

[32] Y. Wu *et al.*, "Understanding the antagonistic effect of methanol as a component in surrogate fuel models: A case study of methanol/n-heptane mixtures," *Combustion and Flame,* vol. 226, pp. 229-242, 2021.

[33] T. Wada, A. Sudholt, H. Pitsch, and N. Peters, "Analysis of first stage ignition delay times of dimethyl ether in a laminar flow reactor," *Combustion Theory and Modelling,* vol. 17, no. 5, pp. 906-936, 2013.

[34] J. Mendes, C.-W. Zhou, and H. J. Curran, "Rate Constant Calculations of H-Atom Abstraction Reactions from Ethers by HȮ2 Radicals," *The Journal of Physical Chemistry A,* vol. 118, no. 8, pp. 1300-1308, 2014/02/27 2014, doi: 10.1021/jp412496g.

[35] H. J. Curran, S. L. Fischer, and F. L. Dryer, "The reaction kinetics of dimethyl ether. II: Low-temperature oxidation in flow reactors," *International Journal of Chemical Kinetics,* https://doi.org/10.1002/1097-4601(2000)32:12<741::AID-KIN2>3.0.CO;2-9 vol. 32, no. 12, pp.

741-759, 2000/01/01 2000, doi: https://doi.org/10.1002/1097-4601(2000)32:12<741::AID-KIN2>3.0.CO;2-9.

[36] U. Burke *et al.*, "An ignition delay and kinetic modeling study of methane, dimethyl ether, and their mixtures at high pressures," *Combustion and Flame,* vol. 162, no. 2, pp. 315-330, 2015/02/01/ 2015, doi: https://doi.org/10.1016/j.combustflame.2014.08.014.

[37] T. Yamada, J. W. Bozzelli, and T. H. Lay, "Comparisons of CBS-q and G2 calculations on thermodynamic properties, transition states, and kinetics of dimethyl-ether + O2 reaction system," *International Journal of Chemical Kinetics,* https://doi.org/10.1002/(SICI)1097-4601(2000)32:7<435::AID-KIN6>3.0.CO;2-4 vol. 32, no. 7, pp. 435-452, 2000/01/01 2000, doi: https://doi.org/10.1002/(SICI)1097-4601(2000)32:7<435::AID-KIN6>3.0.CO;2-4.

[38] Q. S. Li, Y. Zhang, and S. Zhang, "Dual Level Direct ab Initio and Density-Functional Theory Dynamics Study on the Unimolecular Decomposition of CH3OCH2 Radical," *The Journal of Physical Chemistry A,* vol. 108, no. 11, pp. 2014-2019, 2004/03/01 2004, doi: 10.1021/jp037154w.

[39] C. F. Goldsmith, W. H. Green, and S. J. Klippenstein, "Role of O2+ QOOH in low-temperature ignition of propane. 1. Temperature and pressure dependent rate coefficients," *The Journal of Physical Chemistry A,* vol. 116, no. 13, pp. 3325-3346, 2012.

[40] W. Tsang and R. Hampson, "Chemical kinetic data base for combustion chemistry. Part I. Methane and related compounds," *Journal of physical and chemical reference data,* vol. 15, no. 3, pp. 1087-1279, 1986.

[41] G. T. Pullen, P. R. Franke, K. A. Haupa, Y.-P. Lee, and G. E. Douberly, "Infrared spectroscopy of the n-propyl and i-propyl radicals in solid para-hydrogen," *Journal of Molecular Spectroscopy,* vol. 363, p. 111170, 2019.

[42] S. Bai, M. J. Davis, R. Sivaramakrishnan, and R. T. Skodje, "A chemical pathway perspective on the kinetics of low-temperature ignition of propane," *Combustion and Flame,* vol. 202, pp. 154-178, 2019.